NASA/TM-1998-112234

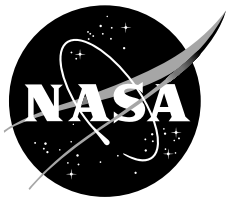

Results of Two-Stage Light-Gas Gun Development Efforts and Hypervelocity Impact Tests of Advanced Thermal Protection Materials

Charles J. Cornelison and Eric T. Watts

October 1998

The NASA STI Program Office . . . in Profile

Since its founding, NASA has been dedicated to the advancement of aeronautics and space science. The NASA Scientific and Technical Information (STI) Program Office plays a key part in helping NASA maintain this important role.

The NASA STI Program Office is operated by Langley Research Center, the Lead Center for NASA's scientific and technical information. The NASA STI Program Office provides access to the NASA STI Database, the largest collection of aeronautical and space science STI in the world. The Program Office is also NASA's institutional mechanism for disseminating the results of its research and development activities. These results are published by NASA in the NASA STI Report Series, which includes the following report types:

- TECHNICAL PUBLICATION. Reports of completed research or a major significant phase of research that present the results of NASA programs and include extensive data or theoretical analysis. Includes compilations of significant scientific and technical data and information deemed to be of continuing reference value. NASA's counterpart of peer-reviewed formal professional papers but has less stringent limitations on manuscript length and extent of graphic presentations.

- TECHNICAL MEMORANDUM. Scientific and technical findings that are preliminary or of specialized interest, e.g., quick release reports, working papers, and bibliographies that contain minimal annotation. Does not contain extensive analysis.

- CONTRACTOR REPORT. Scientific and technical findings by NASA-sponsored contractors and grantees.

- CONFERENCE PUBLICATION. Collected papers from scientific and technical conferences, symposia, seminars, or other meetings sponsored or cosponsored by NASA.

- SPECIAL PUBLICATION. Scientific, technical, or historical information from NASA programs, projects, and missions, often concerned with subjects having substantial public interest.

- TECHNICAL TRANSLATION. English-language translations of foreign scientific and technical material pertinent to NASA's mission.

Specialized services that complement the STI Program Office's diverse offerings include creating custom thesauri, building customized databases, organizing and publishing research results . . . even providing videos.

For more information about the NASA STI Program Office, see the following:

- Access the NASA STI Program Home Page at *http://www.sti.nasa.gov*

- E-mail your question via the Internet to help@sti.nasa.gov

- Fax your question to the NASA Access Help Desk at (301) 621-0134

- Telephone the NASA Access Help Desk at (301) 621-0390

- Write to:
  NASA Access Help Desk
  NASA Center for AeroSpace Information
  7121 Standard Drive
  Hanover, MD 21076-1320

NASA/TM-1998-112234

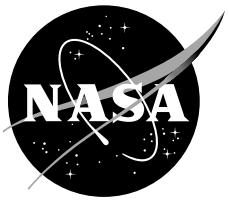

Results of Two-Stage Light-Gas Gun Development Efforts and Hypervelocity Impact Tests of Advanced Thermal Protection Materials

Charles J. Cornelison
Ames Research Center, Moffett Field, California

Eric T. Watts
The Boeing Company, Long Beach, California

National Aeronautics and
Space Administration

Ames Research Center
Moffett Field, California 94035-1000

October 1998

Available from:

NASA Center for AeroSpace Information
7121 Standard Drive
Hanover, MD 21076-1320

National Technical Information Service
5285 Port Royal Road
Springfield, VA 22161

RESULTS OF TWO-STAGE LIGHT-GAS GUN DEVELOPMENT EFFORTS, AND HYPERVELOCITY IMPACT TESTS OF ADVANCED THERMAL PROTECTION MATERIALS

Charles J. Cornelison and Eric T. Watts*

SUMMARY

Gun development efforts to increase the launching capabilities of the NASA Ames 0.5-inch two-stage light-gas gun have been investigated. A gun performance simulation code was used to guide initial parametric variations and hardware modifications, in order to increase the projectile impact velocity capability to 8 km/s, while maintaining acceptable levels of gun barrel erosion and gun component stresses. Concurrent with this facility development effort, a hypervelocity impact testing series in support of the X-33/RLV program was performed in collaboration with Rockwell International. Specifically, advanced thermal protection system materials were impacted with aluminum spheres to simulate impacts with on-orbit space debris. Materials tested included AETB-8, AETB-12, AETB-20, and SIRCA-25 tiles, tailorable advanced blanket insulation (TABI), and high temperature AFRSI (HTA). The ballistic limit for several Thermal Protection System (TPS) configurations was investigated to determine particle sizes which cause threshold TPS/structure penetration. Crater depth in tiles was measured as a function of impact particle size. The relationship between coating type and crater morphology was also explored. Data obtained during this test series was used to perform a preliminary analysis of the risks to a typical orbital vehicle from the meteoroid and space debris environment.

INTRODUCTION

While on-orbit, currently envisioned X-33/RLV vehicles will be exposed to meteoroids and orbital debris. Meteoroids are naturally occurring particles in solar orbit, which are typically comprised of rock and ice-like materials. In contrast, orbital debris is considered to be of man-made origin, such as spent rocket stages, inactive payloads, etc., in Earth orbit. The velocities of these potential impactors vary widely. Meteoroids average approximately 20 km/s and debris particles average 10 km/s (ref. 1). Velocity distributions for meteoroids and space debris are shown in figure 1. Particle sizes cover a wide spectrum from dust specks to large satellites. The smaller sizes are most abundant, whereas larger particles are encountered less frequently. Predicted fluxes based on standard meteoroid and space debris models (ref. 1) are shown in figure 2. Although both meteors and man-made debris contribute to the substantial threat from hypervelocity particle impact, the particles capable of causing critical damage are predominantly man-made debris. Hence, a

* The Boeing Company, formerly Rockwell International

laboratory facility capable of accelerating representative impactor particles to velocities approaching 10 km/s would be ideal for developing an understanding of the effects of orbital debris impact. As of July 1995, the nation's top hypervelocity impact facilities were limited to impact velocities of up to 7 km/s. Thus, the prime motivation for initiating the gun development portion of this project was to expand the velocity envelope for more representative orbital debris impact simulation.

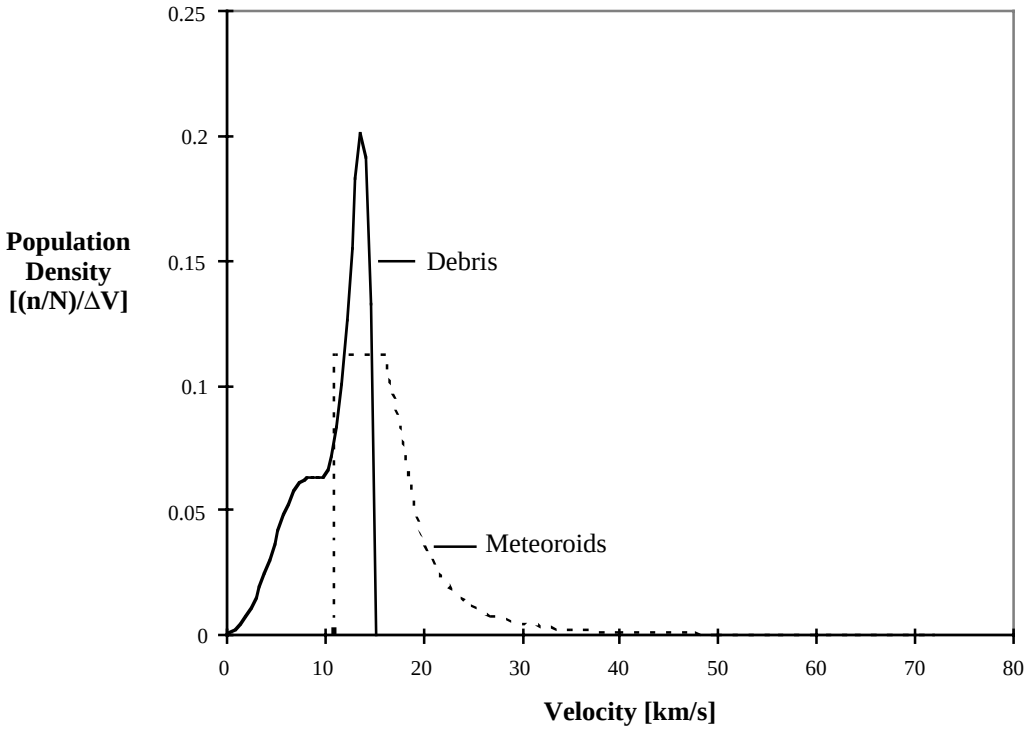

Figure 1. Velocity distribution for meteoroids and space debris.

Despite velocity limitations, hypervelocity impact testing facilities can still provide a useful empirical database of material response. Of particular interest is the material response of a reusable launch vehicle's (RLV's) TPS to orbital debris impact. The survivable damage for an RLV will depend upon both the locations of damage and reentry conditions. Precise determination of survivable damage is beyond the scope of this project. However, computational models of the meteoroid and space debris environments can be combined with material specific impact test data and survivable damage estimates, to predict the overall risk to a vehicle. Thus, the second half of this project was devoted to characterizing the impact damage sustained by various advanced TPS materials from solid particles of sizes and velocities characteristic of the low earth orbit environment.

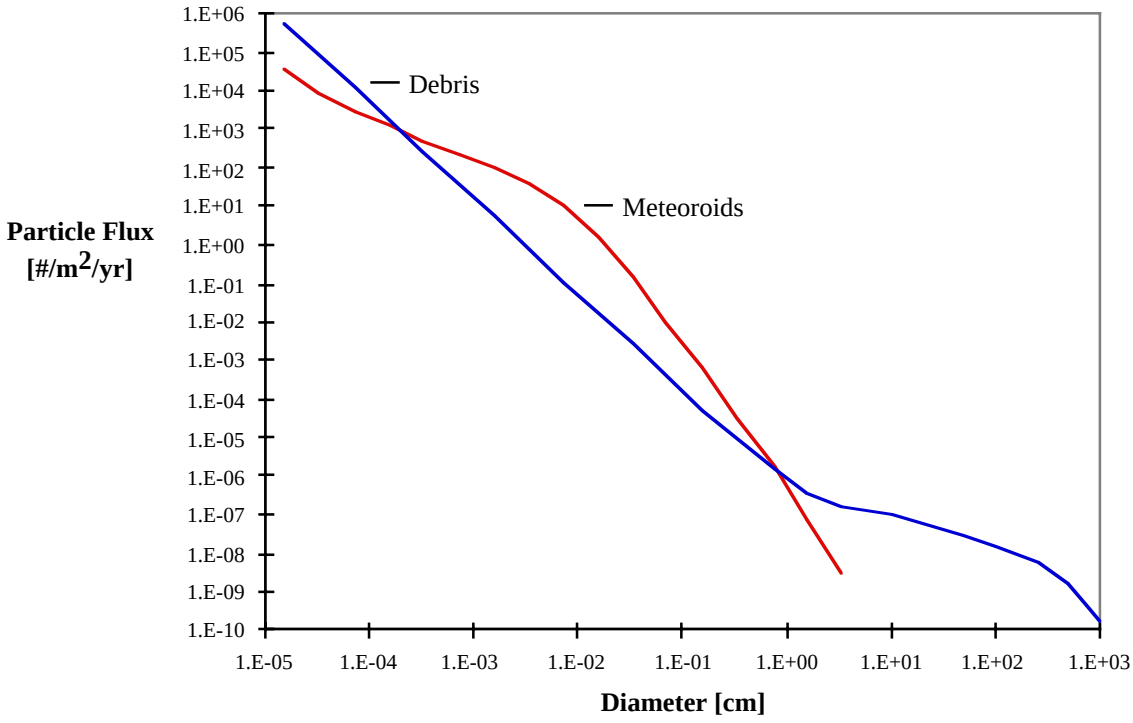

Figure 2. Annual particle flux for meteoroids and space debris.

FACILITY DESCRIPTION

All of the tests discussed in this document were performed in the Hypervelocity Free-Flight Radiation (HFF-Rad) Facility at NASA Ames Research Center (ARC). HFF-Rad is one of two functioning facilities located within the Ballistic Range Complex at ARC. Originally constructed in 1964, the HFF-Rad Facility consisted of a 2-stage light-gas gun; a sabot separation tank; a test section with four orthogonal photo stations; and a shock tube. The purpose of the facility was to launch free-flying models into a counter flowing gas stream to examine (via shadowgraphic, photographic, and spectrographic means) shock layer/gas cap radiation characteristics at extremely high Mach numbers (i.e. M=30). In 1978, the shock tube and test section were removed to allow for the installation of a long path absorption cell facility, which itself was removed in 1992. In 1993, a flight tube and impact chamber were installed (see fig. 3) and the facility was reconfigured to perform impact testing for Johnson Space Center (JSC) in support of the International Space Station Program. During 1995 and 1996 the facility was used for gun development and impact testing for the Reusable Launch Vehicle Program in a collaborative effort with Rockwell International. The results of these two projects are the focus of this document.

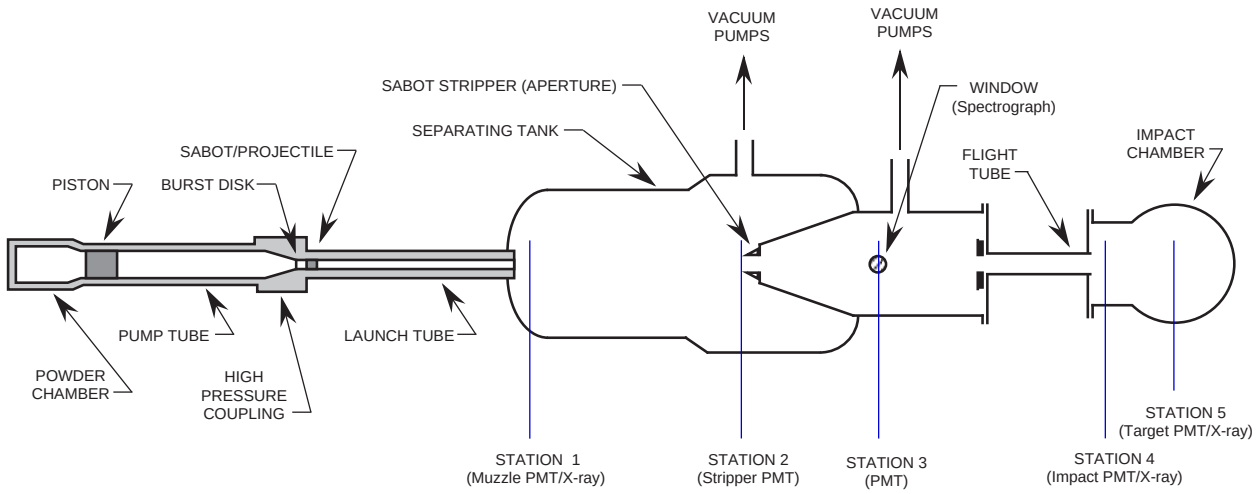

Figure 3. Sectional illustration of the hypervelocity free-flight radiation facility with a typical two-stage light-gas gun.

The facility utilizes an arsenal of three 2-stage light-gas guns: 0.28cal (7.1mm); 0.50cal (12.7mm); and 1.00cal (25.4mm). Using these guns, spherical aluminum particles ranging in size from 1/16-inch (1.59mm) diameter to 3/4-inch (19.05mm) diameter can be accelerated to hypervelocity speeds. There are five photomultiplier tube based time of arrival stations, whose outputs are recorded by digital scopes. Several of the outputs can be used to trigger flash x-ray channels. Details of how a two-stage light-gas gun operates are discussed in reference 2; however, a brief synopsis is as follows. A two-stage light-gas gun typically consists of a powder chamber, pump tube, high-pressure coupling, and launch tube (see fig. 3). A deformable plastic piston is inserted into the upstream end of the pump tube. The sabot (which holds the projectile) is inserted into the launch tube and a burst disk is placed between the high-pressure coupling and launch tube. The pump tube is evacuated and filled with a predetermined amount of hydrogen, and a gun powder charge is placed in the powder chamber. To launch the projectile, the gun powder charge is ignited. The resultant release of chemical energy accelerates the piston, compressing the H_2 gas in the pump tube or first stage of the gun. At a predetermined pressure, the burst disk ruptures and the compressed H_2 gas acts upon the base of the sabot, accelerating it down the launch tube or second stage of the gun. When the sabot and projectile exit the launch tube, they enter the separation tank, wherein the sabot is stripped away from the projectile aerodynamically. The projectile passes through a small aperture, enters the flight tube, and ultimately impacts a target in the impact chamber. During the projectile's flight (from launch tube exit to impact) the shock layer radiation is sensed by each of the photomultipler tubes as the projectile passes by the time of arrival stations. These times are used to calculate projectile velocity.

GUN DEVELOPMENT STUDIES

The initial goal of the gun development effort was to increase the velocity capability of the ARC 0.5-inch (12.7mm) light-gas gun from 6.5 to 8 km/s, while maintaining similar levels of launch tube (gun barrel) erosion, and maximum gun and sabot/projectile base pressures (hence stresses). The reasons for selecting this gun and velocity level were twofold. First, it provides the range of

particle sizes and velocities necessary to support the RLV program requirements. Second, the 0.5-inch gun is the least expensive gun to operate and has the quickest turnaround time of any in the HFF arsenal. The ultimate goal of this ongoing effort is to extend the velocity envelope to 10 km/s, while maintaining acceptable levels of erosion and pressure. How one defines “acceptable” is rather subjective. However, at ARC a standard operating condition must (a) yield at least 20 shots per gun barrel; (b) yield at least 200 shots per high pressure coupling; and (c) produce no projectile deformation upon launch. The total number of shots that can be obtained from a gun barrel is primarily dependent upon the erosion rate. When a gun barrel erodes, the majority of erosion occurs in the first 10 to 20 calibers of length. A taper forms and becomes progressively more pronounced with each shot. Sabots are sized to fit snugly in the first couple of calibers. Thus, as a gun barrel becomes more eroded (hence tapered), the sabot is subjected to increased “radial compression.” Eventually a point is reached wherein either the sabot is unable to survive launch or the projectile impact location becomes too unpredictable. At this point the gun barrel must be changed.

There are many operational parameters that can be varied which affect projectile velocity, gun barrel erosion, and peak pressures in the coupling and at the sabot/projectile base. Some of the most influential parameters are: gun powder mass, gun powder burning rate, piston mass, hydrogen mass, hydrogen compression rate, burst disk rupture pressure, launch mass (sabot plus projectile), and high pressure coupling contraction angle (ref. 3). For example, if one were to gradually increase gun powder mass while keeping all of the parameters constant, one would see a steady increase in projectile velocity with minimal barrel erosion (i.e. $\Delta d/d < 0.1\%$ per shot) up to a critical point. From this point on the erosion would increase dramatically and the velocity would reach a maxima, or plateau. What happens physically is the erosion products (vaporized steel) become entrained in the expanding hydrogen stream. This in turn increases the molecular weight of the flow and reduces the shock speed of the expanding gas. Eventually the point is reached where no matter how much additional gunpowder is used; there is no appreciable gain in velocity. All that results are increased gun barrel erosion and component stress. Conversely, another way to increase velocity is to use a moderate gun powder charge, increase the burst disk rupture pressure, and keep all other parameters constant. This will produce a higher velocity but it will also subject the high-pressure coupling and sabot to pressure peaks that are not only greater in magnitude but sharper as well. In other words, the launch becomes more violent. The likelihood of damaging or destroying the sabot and/or projectile increases, and the longevity of the high pressure coupling decreases. Thus, the trick to elevating the maximum velocity capability is to keep the peak pressures as low and mild as possible, while reducing the erosion rate.

One way to reduce the erosion rate is to reduce the bulk temperature of the compressed hydrogen. This can be accomplished by reducing the hydrogen compression rate, or shortening the length of the pump tube while maintaining the same hydrogen mass. Since the original purpose of the HFF Facilities was to launch delicate aeroballistic models (ref. 2), it's not surprising that the arsenal of light-gas guns were all originally configured to provide a gentle launch capability in the 4 to 6 km/s range. Physically this means the pump tube or compression stroke is too long for optimal high speed impact testing. But how much shortening is optimum, and what about the other parameters? How can one simultaneously reduce the hydrogen temperature and base pressure and yet maximize the projectile velocity? Performing an exhaustive experimental study to correlate all of these parameters would be both time consuming and expensive. As an expedient and cost

effective alternative, a gun performance simulation code was used to perform a parametric study of the aforementioned operating parameters (ref. 3). The product of this study provided a starting point or roadmap of potential parameter adjustments which would lead to attaining the 8 km/s operating condition.

RESULTS AND DISCUSSION

As described in reference 3, the CFD gun performance code was calibrated using the results of numerous tests performed in the 1960s and 1970s. Then for a fixed hydrogen compression rate (pump tube length) and launch mass, the gun powder mass, hydrogen mass, piston mass, and burst disk pressure were varied in such a manner to produce a condition which yielded the highest increases in velocity for the smallest increases in base pressure and hydrogen temperature. This was performed for three different pump tube lengths: 50, 30, and 20 ft (15.24, 9.14, and 6.10 m, respectively). It should be mentioned that during the hydrogen compression phase of the light-gas gun cycle, there is a complex interaction between the conical contraction section of the high pressure coupling and the pressure waves, which coalesce into shock waves and reflect between the advancing piston face and burst disk (prior to rupture). The details of this interaction are beyond the scope of this report, but suffice it to say the code models this complex behavior. Using the code, the optimal wave can be selected for burst disk rupture which minimizes both the peak pressure on the sabot/projectile base, and the pressure induced stresses in the coupling. This is what guides the selection of burst disk rupture pressure. Several high-pressure coupling contraction angles were investigated including those of two existing couplings.

During the experimental test program there were approximately 70 tests performed. Many of these tests were primarily TPS impact tests, some were gun development tests, and some were a combination of both. Combined with these tests were studies to develop the following: (a) more effective and expedient cleaning techniques; (b) optimizing the sabot design to provide minimal launch mass, maximum reliability, and simplified machining; and (c) designing a piston which would fragment minimally, and yet wouldn't extrude excessively making disassembly and clean-up more labor intensive. Table 1 lists representative shots which best exemplify some of the results of the hardware modifications that were implemented. Basically, there were four gun configurations tested: (1) the original 50 ft (15.24 m) pump tube and 7.7° high pressure coupling; (2) a 30 ft (9.14 m) pump tube and 7.7° high pressure coupling; (3) a 20 ft (6.10 m) pump tube and 7.7° high pressure coupling; and (4) a 20 ft (6.10 m) pump tube and 12.5° high pressure coupling. In general, the initial shortening of the pump tube produced a 0.5 to 0.6 km/s increase in velocity. An example of this is a comparison of shots 625 and 627. Further shortening of the pump tube produced an additional 0.2 to 0.3 km/s velocity increase. This is apparent when comparing shots 633 and 650. Switching to the steeper 12.5° coupling produced an additional 0.1 to 0.2 km/s velocity increase, as shown by comparing shots 655 to 663 and 659 to 674. Perhaps the most impressive comparison is between shots 626 and 685. This clearly shows the effects of the fully modified gun configuration. Specifically, the ability to launch 7% more mass to 1.5 km/s higher velocity while maintaining similar erosion levels. Based on several decades of experience, it has been found that for the ARC arsenal of guns, the gun barrel must be replaced once $\Delta d/d$ exceeds 4%. This means that in order to meet the criteria for a standard operating condition the erosion

must be at or below Δd/d = 0.20% per shot. Shot 687 clearly shows that a standard 8.0 km/s condition has been developed for the 0.5-inch gun.

Table 1. Gun development tests, examples of the effects of various hardware modifications.

Shot #	Pump Tube Length (m)	Coupling Angle	Particle Size mm ø	Masses				Burst Disk Pressure (bar)	Velocities		"Δd/d" Erosion at 8 calibers	Shot #
				Launch (gms)	Powder (gms)	Piston (gms)	Hydrogen (gms)		Piston (m/sec)	Projectile (km/s)		
623	15.24	7.7°	6.35	1.406	190	821	8.3	290	768	6.28		623
624	15.24	7.7°	3.18	1.187	195	819	6.5	290	794	7.04	0.18%	624
625	15.24	7.7°	3.18	1.172	195	821	5.3	290	788	7.30	0.22%	625
626	15.24	7.7°	4.76	1.270	187	821	8.3	290	760	6.24	0.10%	626
627	9.14	7.7°	3.18	1.169	195	709	5.3	290	816	7.82	0.40%	627
628	9.14	7.7°	4.76	1.266	197	707	4.1	290	823	8.06	0.40%	628
629	9.14	7.7°	5.56	1.348	195	707	4.9	290	819	7.27		629
633	9.14	7.7°	4.76	1.248	175	719	6.5	290	740	6.50	0.14%	633
637	9.14	7.7°	4.76	1.280	195	720	4.9	290	787	7.53	0.22%	637
643	9.14	7.7°	4.76	1.292	187	717	4.9	310	748	7.21	0.22%	643
650	6.10	7.7°	3.97	1.214	175	720	6.5	310	681	6.71	0.02%	650
655	6.10	7.7°	3.18	1.183	178	718	6.5	310	690	6.81	0.02%	655
659	6.10	7.7°	3.97	1.210	178	714	6.5	310	624	6.42	0.02%	659
663	6.10	12.5°	3.18	1.187	172	718	6.4	310	664	7.00	0.02%	663
674	6.10	12.5°	3.18	1.200	173	717	6.4	310	655	6.53	0.02%	674
675	6.10	12.5°	3.97	1.214	175	718	5.3	310	657	7.14	0.04%	675
682	6.10	12.5°	1.59	1.184	173	717	6.2	310	687	6.98	0.02%	682
683	6.10	12.5°	5.95	1.400	180	717	4.9	310	690	7.44	0.12%	683
685	6.10	12.5°	5.56	1.348	195	716	4.9	310	693	7.71	0.10%	685
687	6.10	12.5°	5.56	1.356	215	711	4.9	310	748	8.05	0.14%	687

TPS IMPACT STUDIES

Advanced TPS materials, under development for potential use on an RLV such as the X-33, were characterized with respect to impact from space debris. Utilizing the NASA Ames 0.5-inch light-gas gun, ceramic based TPS materials were impacted with aluminum spheres ranging in size from 1/16- to 9/32-inch (1.59 to 7.14 mm) diameter at velocities in the range of 6-8 km/s. The 1/16-inch (1.59 mm) diameter spheres were 2024-T3 aluminum, all others were 1100-O aluminum. Materials tested include AETB-8, AETB-12, AETB-20, and SIRCA tiles (ref. 4), TABI, and HTA (ref. 11). In general, the target specimens were comprised of a 15.2 cm x 15.2 cm TPS coupon bonded to a 25.4 cm x 25.4 cm structural substrate. A "witness plate" made of 2024 T3 aluminum, 25.4 cm x 25.4 cm with 12.7 mm thickness was held 6.4 cm behind each specimen during testing to characterize any particles passing through the target. However, impact conditions were selected to create, at most, threshold penetration. Thus, no cratering occurred in any of the witness plates. Some TPS materials were bonded to composite panels which represented an RLV "intertank" region. The composite panels were fabricated using laminated IM-7 graphite/5250-4 Bismaleimide resin (BMI) by Cytec Engineered Materials Inc. These "skins" were 12-ply and had a nominal thickness of 0.070 in. (1.78 mm). BMI composite panels were the baseline substrate for ballistic limit tests. A 2024-T81 aluminum substrate was used where comparison with Space Shuttle

Orbiter data was of interest, and 2024-T0 aluminum was used where no impact of the substrate was expected. A simple test fixture was devised to clamp the target specimen along its perimeter edges, thereby minimizing recoil deflection.

Several combinations of tile substrates and coatings were investigated. Alumina Enhanced Thermal Barrier (AETB) tiles, in nominal 8, 12, and 20 lbs/ft^3 (0.13, 0.19, and 0.32 g/cm^3) densities, were fabricated per specification (ref. 4) at Rockwell's Advanced Manufacturing Laboratory in Downey, California. The AETB material contains alumina, silica, and aluminoborosilicate fibers. Silicone Impregnated Reusable Ceramic Ablator (SIRCA) was made from LI-2200, the high density Orbiter tile substrate, using a NASA Ames process (ref. 7). In this process the entire LI-2200 tile is densified with RTV silicone, which forms a coating around the tile fibers. The resulting TPS material had a nominal density of 25 lbs/ft^3 (0.40 g/cm^3). Coatings investigated include Reaction Cured Glass (RCG), Toughened Unipiece Fibrous Insulation (TUFI), the combination TUFI with RCG (TUFIR), and a concentrated TUFI coating (TUFIC). All coatings were sprayed on AETB tiles per specification (ref. 5) except that the weight of TUFI was applied at 0.17 g/cm^2 (rather than the standard 0.12 g/cm^2). Nominal coating weights were 0.08 g/cm^2 for RCG, 0.17 g/cm^2 for TUFI and TUFIC, and 0.22 g/cm^2 for TUFIR. RCG is a black glass composed of borosilicate glass frit, silicon tetraboride. The TUFI coatings are made of borosilicate glass frit, molybdenum disilicide, and silicon hexaboride. The TUFI coating penetrates into the top ~2 mm of the tile surface forming a densified, porous layer. TUFIC also penetrates the tile surface but forms a nearly non-porous coating. The RCG coating in contrast forms a continuous coating which sits on top of the tile substrate. The tiles were bonded to substrates utilizing a 0.090 in. (2.29 mm) strain isolator pad (SIP) and RTV silicone adhesive (ref. 6). Figure 4 depicts a typical coated tile target specimen.

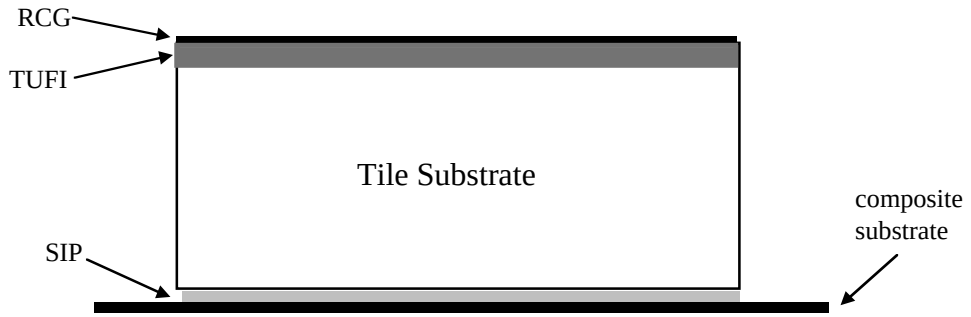

Figure 4. Cross-section of a typical coated tile test specimen.

Two types of blankets were investigated during this test series: (1) TABI, which is a relatively new blanket under development by NASA Ames and Rockwell (now Boeing); and (2) HTA, which is based on the quilted architecture of the Orbiter advanced flexible reusable surface insulation (AFRSI). Figure 5 shows a schematic depiction of the two blanket architectures. The woven TABI structure, nominally 1.2 inches (3 cm) thick, was filled with processed alumina batting using current laboratory procedures (ref. 8). The assembly was heat cleaned (ref. 9) prior to coating. Thick blanket specimens of 2 and 3 in. (5.1 and 7.6 cm) nominal thickness were fabricated by stacking TABI on 1 and 2 in. (2.5 and 5.1 cm) HTA blankets, respectively. Stacked blankets were

secured using “cinch” knots; one of several potential methods for joining blankets (ref. 10). HTA blankets were fabricated according to the Orbiter blanket specification (ref. 11), but with higher temperature fibrous insulation, thread, and outer mold-line (OML) fabric. The fibrous insulation was alumina based Saffil, the thread was Nextel-440, and the OML fabric was 3-ply angle-interlock Nextel-440. Both blanket types were coated with a sprayable ceramic outer refractory (SCOR) coating (ref. 12) and waterproofed (ref. 13) in accordance with Rockwell specifications. Blanket target specimens were simply cut from larger production units and bonded to the BMI composite substrate (ref. 14).

Figure 5. TABI’s integral woven fabric channels (left) and HTA’s stitched, quilted construction are shown schematically.

RESULTS AND DISCUSSION

The test results of individual hypervelocity impacts are listed in Appendix A. Data include shot parameters, penetration versus no penetration, crater depth, and a description of the damaged specimen. Primarily, TPS test specimens were characterized with respect to impact crater size and ballistic limit. These damage levels were selected as a basis for covering critical damage to a thermal protection system. Critical damage is defined as a level of damage which would result in the loss of a vehicle. Defining critical impact damage to a reusable launch vehicle bears heavily on the severe reentry environment. As a first approximation and as is assumed for the lower surface of the Orbiter, a through penetration of the TPS and structure may be considered critical damage. However, depending on the reentry profile, damage location, and other vehicle specific parameters, a crater in the TPS may cause burn-through and hence constitute critical damage. This is the case in the Orbiter Program where critical damage to the wing leading edge is defined as a crater into the Reinforced Carbon-Carbon (RCC) composite. Materials characterization, to determine particles which may cause critical damage (critical particles), can be used to support analysis to determine vehicle risk resulting from the meteoroid and space debris environment. The detailed analysis required to define critical particles and risk for an RLV type vehicle is beyond the scope of this project. However, a simplified risk calculation is presented later in this section in order to illustrate the significance of the problem.

The ballistic limit, although well defined for metallic targets, remains qualitative for composite materials. This is due to the damage mechanisms associated with impacts to composite laminates. In metals, the ballistic limit is defined as the threshold at which rear surface “spall” material becomes detached and a clear perforation exists through the target. In composite laminants however, the point of through penetration is not clear. Rear surface damage progresses from individual ply de-laminations to broken fibers and matrix removal. Matrix fracturing and removal is a fairly continuous process and the integrity of an impacted composite laminant may be compromised before a visible through penetration exists. Furthermore, the integrity of a composite

panel must be defined based on the use of the material, and will be different for a pressure vessel than a TPS material substrate. Future work must consider, for example, the effect of the re-entry plasma environment on damaged TPS/composite systems and the threshold damage for pressurized composite tanks. For this program a penetration was defined as the point at which light could be seen through the damaged laminant. Visually, this appears as “pin holes” of light through a thick mass of splintered fibers and matrix. This level of damage is more severe than the threshold at which gas flow would occur through the damage site, different than the ballistic limit for metallic targets.

Initially, several tests were devoted to investigating ballistic limit as a function of impact velocity. AETB-12 TUFI coated tiles were impacted with aluminum spheres at velocities between 6 and 8 km/s. Figure 6 shows the results of these tests. Over this velocity range and for the limited number of test shots available, no significant dependence of ballistic limit on velocity was observed. Subsequent tests were performed at 6.5–7.0 km/s to minimize facility maintenance. AETB-8 tile/substrate was the focus of additional ballistic limit testing. Figure 7 is a plot of test data indicating the range of the ballistic limit of tile/substrate systems. Impact velocities were in the range 6.2–8.1 km/s. In this test program, no differences in ballistic limit were observed for different coatings and figure 7 incorporates data from both TUFI and TUFIR coated tiles. The relatively large ballistic limit ranges are due to the 1/32-inch (0.79 mm) particle size resolution and limited number of test shots available and are expected to encompass the ballistic limits of the tile systems independent of coating. Figure 7 also identifies the improved penetration resistance of AETB-12, with respect to AETB-8, due to its greater density. The ballistic limit for a typical Orbiter system, determined during previous Rockwell testing is also shown. The Orbiter system consisted of RCG coated LI-900 on 0.1-in. (2.54 mm) 2024-T81 aluminum. The improved ballistic limit of the Orbiter system is due to the higher density aluminum substrate. No direct tile comparison is possible.

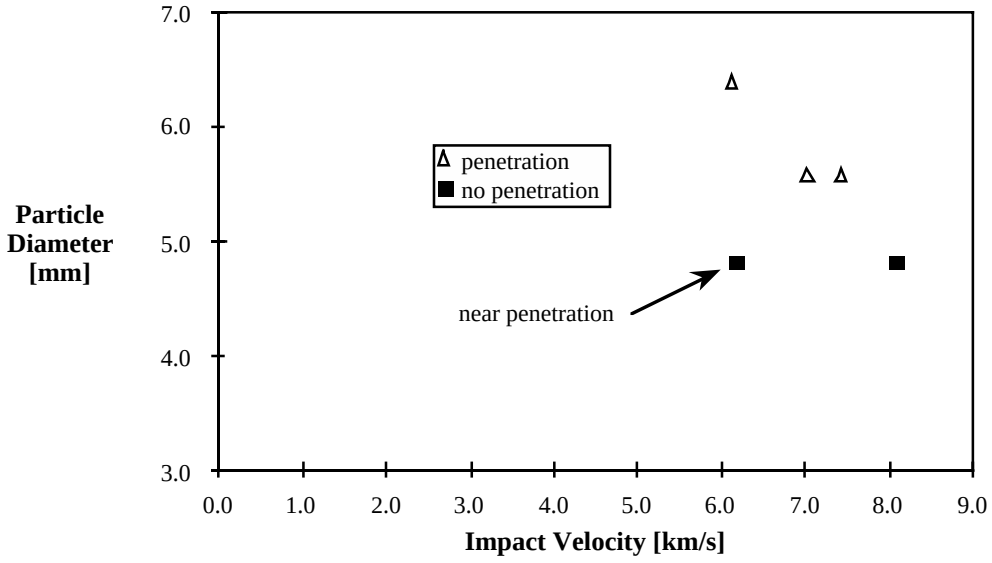

Figure 6. Limited data shows no significant velocity dependence of ballistic limit for TUFI coated 2 in. (5.1 cm) AETB-12 tiles on 0.070 in. (1.78 mm) BMI substrate.

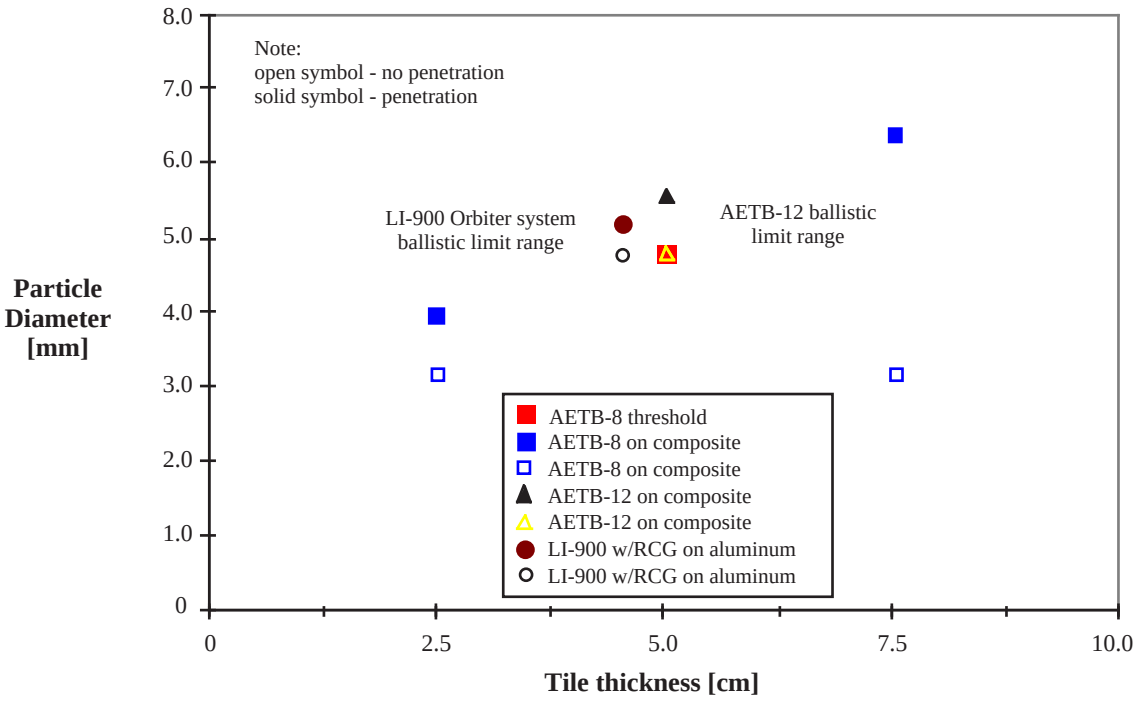

Figure 7. Ballistic limits which lie between shots of penetration and no-penetration are empirically mapped for advanced and Orbiter tile/structure systems.

Figure 8 presents a plot of the maximum penetration depth into various tile/coating systems versus impact particle size. During this test program, the baseline coating for Rockwell's X-33 vehicle was changed from TUFI to TUFIR. Data are shown for both coatings on AETB-8. Some reduction in crater depth may result from the heavier TUFIR coating. Crater depth in TUFIC coated AETB-20 and SIRCA-25 are also shown in the figure. The results show the expected reduction of crater depth with increasing TPS density. Impact velocities were in the range 6.4–7.3 km/s.

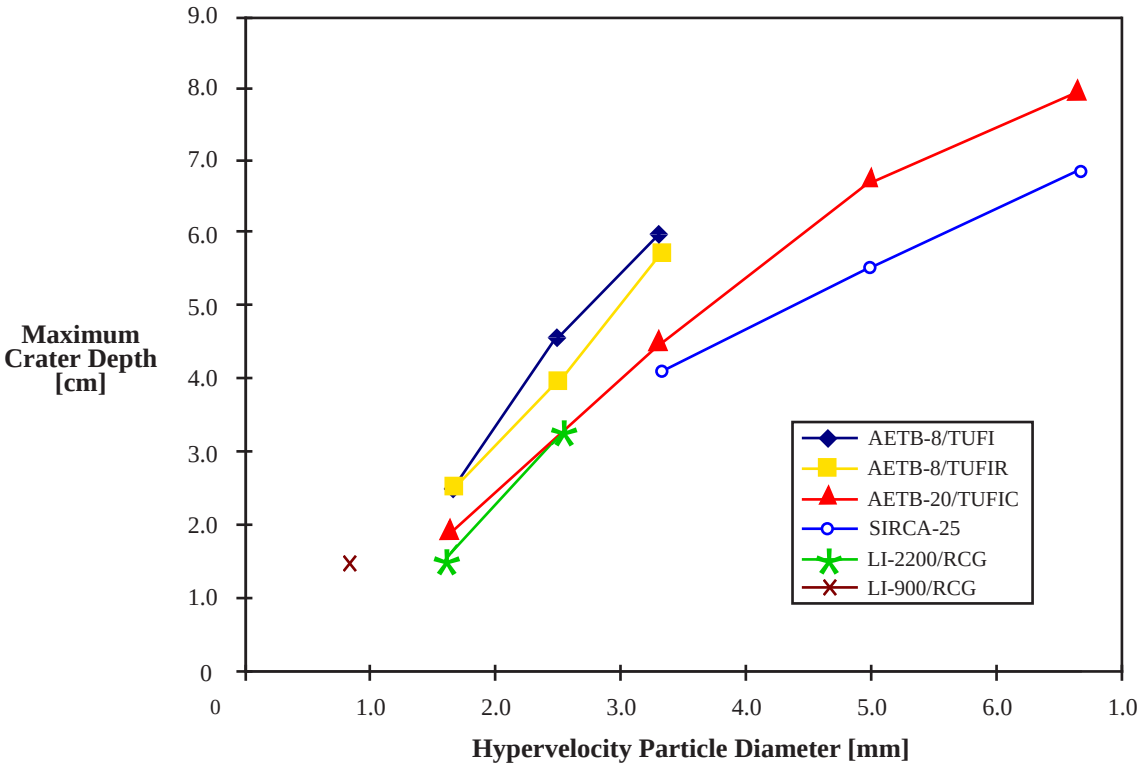

Figure 8. Crater depths for TPS tiles impacted at 6.6 ± 0.1 km/s.

Impact craters were characterized by several measurements as shown in figure 9. The maximum penetration depth was measured as the deepest pit extending below the crater opening. In general, craters have a fairly symmetrical shape and an "average" crater depth was measured to suggest this. Entrance holes were approximately circular and an "average hole diameter" was estimated to describe the throat of the cavity. Coating spall was also measured. Selected tile craters, which were to be repaired and/or further studied, were imaged via computed X-ray tomography and these are presented in figure 10. The figure shows craters in uncoated AETB-20, TUFIC coated AETB-20 and SIRCA-25 resulting from impact of 1/8-inch (3.18 mm) aluminum spheres at 6.8, 6.9, and 7.3 km/s, respectively. Craters are shown left to right. The projectile/coating impact interaction has been described as significant in the breakup of the impacting particle (refs. 15 & 16). On impact, the particle breaks up to some extent depending upon the peak shock pressure generated at initial impact. Note that the uncoated tile crater is the most symmetrical, while the SIRCA tile and TUFIC coated AETB-20 tile craters have large subcraters extending below the main cavity. This seems to indicate the presence of larger particle fragments, which would have caused the "sub craters." Very limited data makes conclusions difficult. However, X-ray computed tomography may be a useful for crater analysis where destructive analysis is not acceptable.

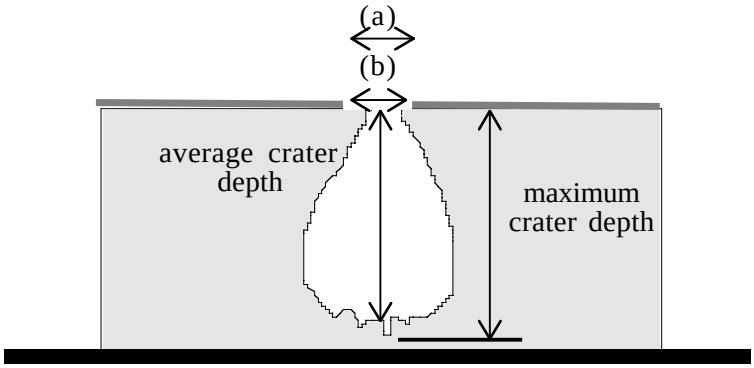

Figure 9. Measurements performed on hypervelocity impact craters in tile include coating spall (a) and entrance hole diameter (b).

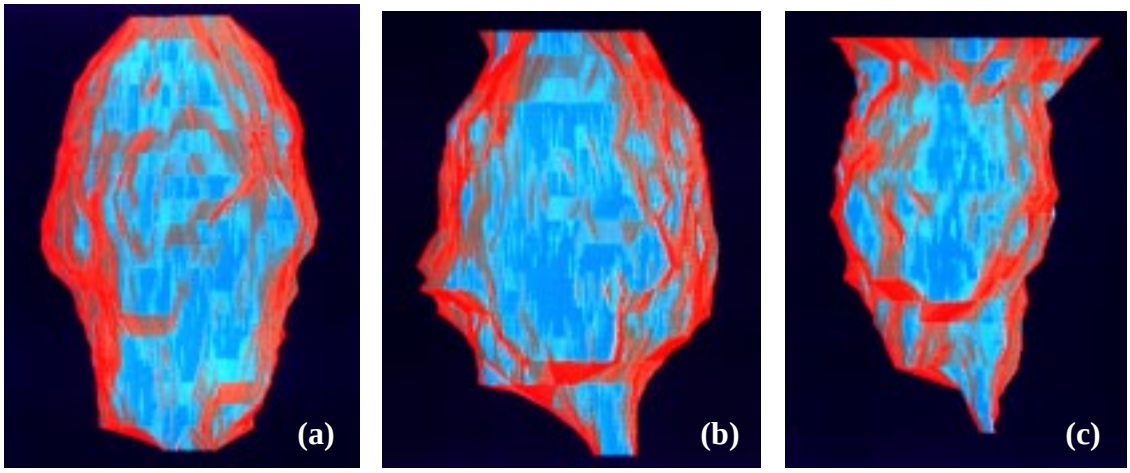

Figure 10. Computed Tomography images (1.25x) of impact craters reveals subtle differences in (a) uncoated AETB-20, (b) TUFIC coated AETB-20, and (c) SIRCA tiles.

Comparisons were made of crater dimensions for several coatings on AETB-8 and AETB-20. Measurements were performed on AETB-8 tiles shot with 1/16-inch (1.59 mm) aluminum spheres with an impact velocity of 6.65 ± 0.15 km/s. The results are presented in figure 11. Figure 12 shows crater dimensions for AETB-20 tiles shot with 1/8-inch (3.18 mm) spheres at 6.85 ± .05 km/s. Comparison of coated and uncoated tiles supports previous observations that coatings serve to break up the impacting particles resulting in shallower impact craters. The maximum penetration depth into the uncoated AETB-8 tile was ~33% deeper than the crater in the TUFIR coated tile. The crater in uncoated AETB-20 was only ~8% deeper than the TUFIC coated tile. This is significantly less than has been reported for LI-2200, used in the Orbiter program. Previous hypervelocity tests compared uncoated and RCG coated LI-2200 and found a 30% increase in crater depth in the uncoated tiles (ref. 15). This discrepancy points toward the need for developing statistics on hypervelocity impact test results through correlation of multiple shots (the above comparison is between two single test points). The TUFI, TUFIR, and TUFIC coatings, which

penetrate the tile surface and form a dense layer of increased strength, also result in larger entrance holes. Although the penetration depths into the coated tiles are fairly uniform, the differences in hole diameter may play a roll in reentry heating survivability. Although not indicated on this figure, it was observed that the RCG bonds more securely to a TUFI coated tile surface than it does directly to AETB. The RCG layer did not debond from the TUFI surface as it did when coated directly on the AETB surface. Figure 13 compares craters in TUFIC coated AETB-20 and SIRCA-25 impacted by 1/8-inch (3.18 mm) spheres at 7.3 km/s. The SIRCA material is seen to have a shallower crater, but also significantly more material is spalled from the front surface of the tile (see fig. 10).

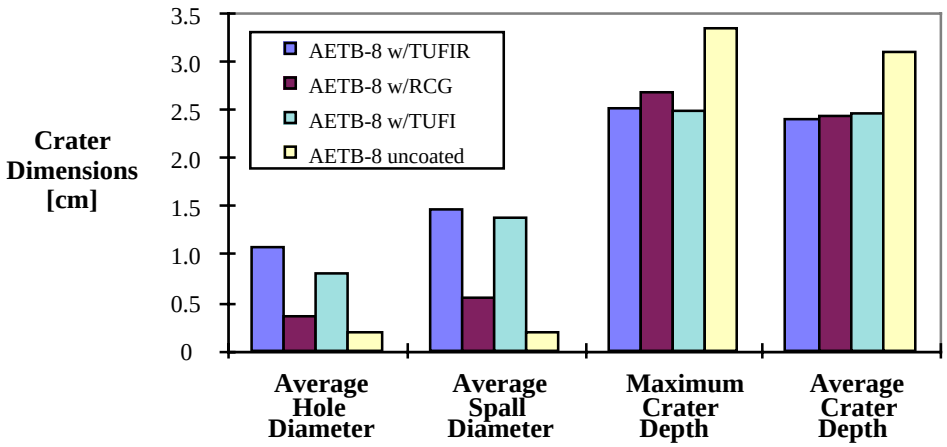

Figure 11. Crater dimensions for AETB-8 tiles impacted with 1/16-inch (1.59 mm) spheres.

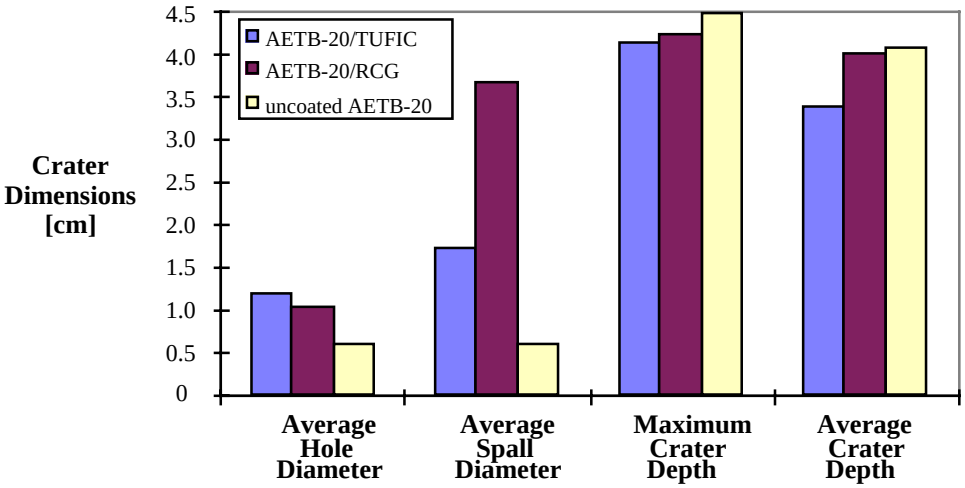

Figure 12. Crater dimensions for AETB-20 tiles impacted with 1/8-inch (3.18 mm) spheres.

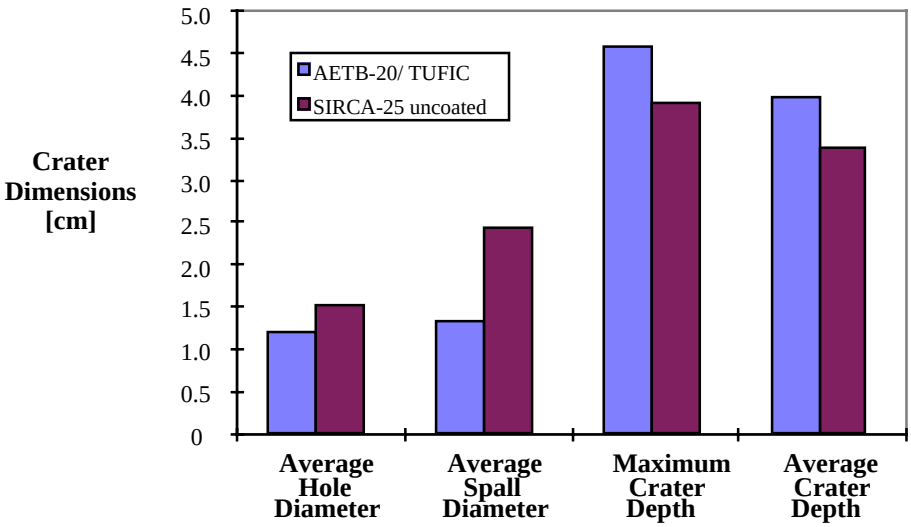

Figure 13. Crater dimensions for AETB-20 and SIRCA-25 tiles impacted with 1/8-inch (3.18 mm) spheres.

A comparison of the amount of material penetrated is useful in understanding the protection per unit weight offered by the various tile materials. Figure 14 shows that on a "per-unit-weight" basis the tile coatings, which are necessary to protect against other environment impacts (refs. 16 & 17), do not increase the effectiveness of stopping hypervelocity particles. Figure 15 summarizes these results, and shows the best protection per weight to be the lowest density tile system, AETB-8. The differences in coating, however, are not significant. For the high-density tiles, SIRCA performed better than AETB-20, perhaps due to energy ablated during impact due to its organic silicone impregnation. As a point of reference, the figure also presents the expected penetration into aluminum.

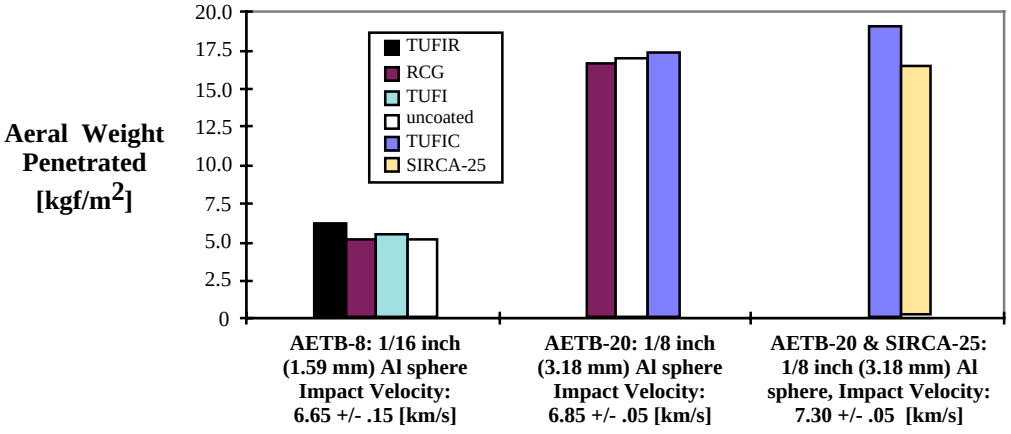

Figure 14. Coatings have minor affect on penetration resistance per unit weight.

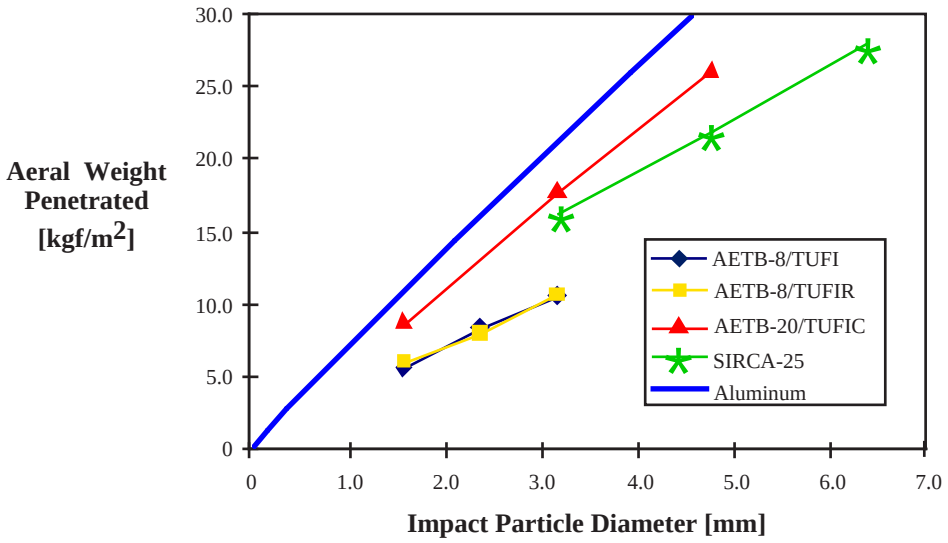

Figure 15. TPS material penetration resistance characterized by weight penetrated. Note: (Aeral Weight Penetrated) = (material density) x (penetration depth).

Ballistic limits were investigated for several blanket/structure systems. As with the tile ballistic limit shots, 0.070 in. (1.78 mm) BMI composite was used as the substrate. Coated and uncoated 1 inch (2.5 cm) HTA blankets and 1.2 inch (3 cm) coated TABI blankets were shot with various sizes of aluminum spheres to define the range of the penetration threshold. Once again, the threshold or ballistic limit lies between two shots – one that penetrates and one that does not penetrate. Table 2 lists blanket ballistic limit shot parameters and results. Several additional shots were used to evaluate impacts to thicker TABI blanket systems. Nominally 1 in. (2.5 cm) thick TABI blankets were stacked on 1 and 2 in. (2.5 and 5.1 cm) HTA blankets to produce 2 and 3 in. (5.1 and 7.2 cm) blanket systems, respectively. Damaged blankets were to be exposed to plasma arcjet simulated reentry conditions to determine survivable damage, however, program complications precluded this effort. Table 3 lists test parameters and results for thick TABI blankets. Small entrance holes were observed on all blanket impacts and the fabric surface was largely unchanged except for the entrance hole. A small amount of coating spall was lost around the entrance hole. Within the blanket, as with tiles, a large cavity was present (although not completely devoid of insulation material). Stacked TABI blankets (table 3) were separated at the blanket/blanket joint and the interface was examined. The 1/16-inch (1.59 mm) particle was completely stopped within the 1.2 in. (3 cm) TABI blanket, only minor discoloration was visible on the rear TABI fabric. The 1/8-inch (3.18 mm) particle caused a ~0.6 in. (15.2 mm) diameter hole through the TABI rear fabric and through the underlying HTA blanket down to the composite substrate. No rear surface damage to the substrate was visible. A similar result was obtained from the 5/32-inch (3.97 mm) particle except the hole through the TABI/HTA blanket “stack” was ~1.0 in. (2.5 cm) in diameter. Again, no visible rear surface damage to the composite substrate was visible.

Table 2. Hypervelocity impact test shots used to bracket blanket ballistic limits.

Target Specimen	Velocity (km/s)	Particle Dia. (mm)	Result
2.5 cm SCOR coated HTA on 1.78 mm BMI	6.7	1.59	no penetration
2.5 cm SCOR coated HTA on 1.78 mm BMI	6.8	2.38	barely penetrated @ threshold
2.5 cm uncoated HTA on 1.78 mm BMI	6.6	1.59	no penetration
2.5 cm uncoated HTA on 1.78 mm BMI	6.7	3.18	penetrated - 10 mm exit hole
3.0 cm SCOR coated TABI on 1.78 mm BMI	6.3	2.38	no penetration
2.7 cm SCOR coated TABI on 1.78 mm BMI	6.5	3.18	penetrated

Table 3. Stacked TABI blanket impact test results.

Target Specimen	Velocity (km/s)	Particle Dia. (mm)	Entrance Hole (mm)	Coating Spall (mm)
5.3 cm TABI w/SCOR coating on 1.78 mm BMI	6.4	3.97	4.8	9.5 x 11.1
5.5 cm TABI w/SCOR coating on 1.78 mm BMI	6.8	3.18	4.8	9.5 x 12.7
7.2 cm TABI w/SCOR coating on 1.78 mm BMI	6.7	1.59	1.6 x 3.2	6.4 x 9.5

Characterization of spacecraft materials with respect to impact from hypervelocity particles is a necessary step towards understanding the resistance of these materials to the meteoroid and space debris environment. The application of hypervelocity impact characterization data comes in the analysis of spacecraft risk. The risk of impact from meteoroids and space debris can range from subtle changes in surface optical properties to a complete loss of space system function. For thermal protection materials, meteoroid or space debris impact damage can result in the catastrophic loss of the reentry vehicle.

To put into perspective the risk associated with the meteor and space debris environment and the characterization data obtained during these tests, an analysis was made of a hypothetical reusable launch vehicle program. For this purpose, an RLV geometry was defined based on Rockwell's winged-body X-33 design baseline (circa 1996). Most simply, this design is a cylinder with wings. Hence, for this analysis a "vehicle" has been defined as a cylinder 176 feet (53.6 m) long and 35 feet (10.7 m) in diameter (ref. 19). Neglecting the area of the wings and cylinder ends, the flux of particles impacting this "vehicle" for meteoroids and space debris was calculated based on standard models (ref. 1). For this analysis the environment was (conservatively) fixed for the year 2000, using the typical 5% growth rate in debris flux. Probability calculations were then performed for a fleet of 5 vehicles, each making 100 three-day space station re-supply missions (354 km, 51.6° inclination). Figure 16 presents the results of this analysis as the impact probability, or risk, of one or more impacts of a given size particle. In this study, particles causing threshold

penetration ranged from 0.02 to 0.375 grams, for 1 in. (2.5 cm) coated blankets, and 3 in. (7.6 cm) coated tiles on composite structures, respectively. These material systems modeled the TPS/intertank region of an RLV. Other work has been done to investigate hypervelocity impact to various RLV TPS/fuel tank configurations, and has found particles causing threshold penetration to be in the range 0.047 to 0.74 grams (ref. 21). Detailed analysis has shown particles capable of causing critical damage to the Space Shuttle Orbiter are in the range of $1x10^{-1}$ to $5x10^{-1}$ grams (ref. 20). It is clear from a comparison of penetrating particle size and figure 16 that the risk of a critical impact over the lifetime of an RLV program is substantial.

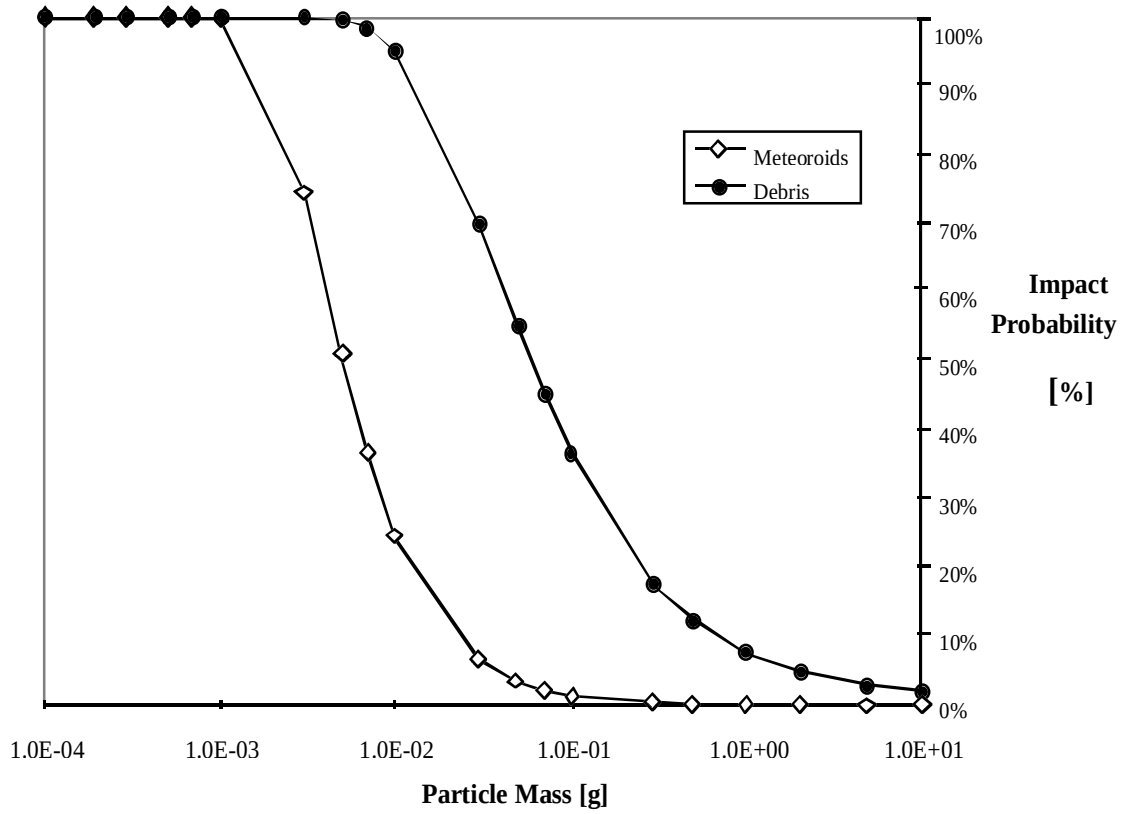

Figure 16. Probability of one or more impacts of a given mass over the duration of an RLV "program" (5 vehicles and 100, 3-day missions per vehicle).

CONCLUSIONS

Gun development efforts to increase the launching capabilities of NASA Ames 0.5-inch (12.7 mm) two-stage light-gas gun were investigated. Using a gun performance code as a starting point, the operational parameters and gun hardware were varied, in order to increase projectile impact velocity capabilities. Specifically, the 0.5-inch gun is now able to launch 7% more mass to 1.5 km/s higher velocity while maintaining similar levels of gun barrel erosion and gun component stresses. A usable 8 km/s operating condition now exists for the full spectrum of particle sizes (1/16- to 9/32- inch or 1.59 to 7.14 mm diameter), and there appears to be potential for further velocity increases.

Concurrent with the facility development effort, a hypervelocity impact testing series in support of the X-33/RLV program was performed in collaboration with Rockwell International (now Boeing). Advanced thermal protection system materials were impacted with aluminum spheres to help define their response to impact from orbital debris. Materials tested included AETB-8, AETB-12, AETB-20, and SIRCA tiles, TABI, and HTA. The ballistic limit for several material systems was investigated to determine particle sizes which cause TPS/structure penetration. Not surprisingly, the ballistic limit was found to increase with tile density and blanket thickness. Crater depth in tiles was measured as a function of impact particle size. It was observed that coatings, which serve to shock and break up the impacting particle, increase the penetration resistance of a given thickness of tile. However, there is a weight tradeoff and the best protection per unit weight of material is not from the heaviest coating. No coating and the lightest coating, RCG, performed better in this respect. The most significant difference between the craters formed in tiles with different coatings was the size of the entrance hole and spall region. Such differences in crater morphology may have an effect on reentry heating survivability.

Finally, test data was compared to an analysis of impact risk to a hypothetical reusable launch vehicle program. Based on this first order analysis, it is clear that the worsening space debris environment poses a very real threat to future manned space missions. Additional work is required to adequately characterize available advanced spacecraft materials. Specifically, the survivability of impact damaged TPS should be determined for advanced systems by combined hypervelocity impact and plasma arcjet testing. Proposed systems include the use of composite structures and substrates which will respond inherently different than metallics, both to particle impact as well as to the reentry environment. Future programs will also require development of some level of statistics on hypervelocity impact test results. In order to adequately protect our space investments and ensure the security of our astronauts, this area of research warrants further investigation.

ACKNOWLEDGEMENTS

The authors would like to acknowledge the invaluable contributions and dedication of the Ballistic Range Complex operating crew, Don Bowling and Don Holt. We also would like to acknowledge the computational support provided by Dr. Dave Bogdanoff, and the instructive comments and useful suggestions provided by John Balboni and Mark Newfield.

REFERENCES

1. J. Anderson, Ed. and R. Smith, Compiler, Natural Orbital Environment Guidelines for Use in Aerospace Vehicle Development. NASA TM-4527, 1995.

2. T. N. Canning, A. Seiff, and C. S. James, Ballistic Range Technology, AGARDograph No. 138 (1970).

3. D.W. Bogdanoff, Optimization Study of the Ames 0.5-inch Two-Stage Light-Gas Gun, NASA TM-110386 (1996).

4. Rockwell Process Specification, Rigid Thermal Protection Material Fabrication, MA0614-003.

5. Rockwell Process Specification, Coating Process for TUFI and TUFIR Coatings: MA0606-326, Coating Process for TUFIC: MPLP 284-400-96-002.

6. Rockwell Process Specification, Process for Bonding Rigid TPS Materials, MA0106-319.

7. NASA Material Processing Specification, Processing of Silicone Impregnated Ceramic Ablator.

8. Tina Lu, Rockwell TABI Processing Specification: MPLP-284-400-96-051 (1996).

9. NASA Heat Processing Specification, Heat Cleaning of High Temperature Ceramics, 9SP-90001-XR16.

10. R. Reynolds, Rockwell Laboratory Test Report, LTR-6766-4049, "Methods for Blanket-to-Blanket Attachment" (1996).

11. Rockwell Production Specification, Production of Reusable Flexible Surface Insulation, MBO135-085.

12. Rockwell Process Specification, Process for Sprayable Ceramic Outer Refractory Coating, MPLP284-400-96-014.

13. Rockwell Process Specification, Process for Waterproofing Reusable Flexible Surface Insulation, MAO608-306.

14. Rockwell Process Specification, Process for Bonding Reusable Flexible Surface Insulation, MA0606-317.

15. E. Christiansen and J. Ortega, "Hypervelocity Impact Testing of Shuttle Orbiter Thermal Protection System Tiles," AIAA Paper No. 90-3666.

16. Eric Christiansen, Evaluation of Space Station Meteoroid/Debris Shielding Materials, Eagle Engineering Report No. 87-163 (1987).

17. E. T. Watts, Low Velocity Impact Testing of Advanced Thermal Protection System Materials, Rockwell International Space Systems Division Laboratory Test Report, LTR-6770-4051, September 1996.

18. E. T. Watts, Rain Impact Fight Testing of Advanced Thermal Protection System Materials, Rockwell International Space Systems Division Laboratory Test Report, LTR-6815-4030, June 1996.

19. S. Greenberg, Requirements Report for SSTO Vertical Take-off/Horizontal Landing Vehicle, Rockwell International Report, SSD-94-D0217A (1994).

20. M. Hasselbeck, et. al, Orbiter Space Particle Impact Hazard Study, Rockwell International Engineering Report, SSD-91-D0771 (1991).

21. J. Robinson, A. Nolan, et. al., “Meteoroid/Orbital Debris Implications to a Reusable Launch Vehicle Thermal Protection System,” AIAA Paper 95-3606.

APPENDIX A. HYPERVELOCITY IMPACT TEST SHOTS

Test parameters and target descriptions are summarized below for all of the TPS Impact shots performed under this program.

Shot #	ID#	Target Description	Coating	Damage Description
661	HVTT-1	3in. (7.62cm) AETB-8 / .07in. (1.78mm) BMI	TUFI	pen.- tile separated from skin above SIP/2.5cm of broken fibers
678	HVTT-2	3in. (7.62cm) AETB-8 / .07in. (1.78mm) BMI	TUFI	crater
680	HVTT-2	3in. (7.62cm) AETB-8 / .07in. (1.78mm) BMI	TUFI	crater
633	HVTT-3	2in. (5.08cm) AETB-8 / .07in. (1.78mm) BMI	TUFI	no pen., bump & fiber separ. on rear, fractured @ bond line
634	HVTT-4	2in. (5.08cm) AETB-8 / .07in. (1.78mm) BMI	TUFI	no pen., slight bump & fiber separ. on rear, fractured @ bond line
637	HVTT-6	2in. (5.08cm) AETB-8 / .07in. (1.78mm) BMI	TUFI	pen.-pinholes, broken & peeled fibers on rear, fractured @ bond line
638	HVTT-7	1in. (2.54cm) AETB-8 / .07in. (1.78mm) BMI	TUFI	pen.-12.7mm dia., broken & peeled fibers on rear
639	HVTT-8	1in. (2.54cm) AETB-8 / .07in. (1.78mm) BMI	TUFI	no pen., bump & fiber separ. on rear
623	HVTT-9	2in. (5.08cm) AETB-12 / .07in. (1.78mm) BMI	TUFI	pen.-9.5mm,broken & peeled fibers on rear, fractured @ bond line
628	HVTT-10	2in. (5.08cm) AETB-12 / .07in. (1.78mm) BMI	TUFI	no pen., no bumps, no fractures
629	HVTT-11	2in. (5.08cm) AETB-12 / .07in. (1.78mm) BMI	TUFI	pen.-3.2mm, broken & peeled fibers on rear, fractured @ bond line
626	HVTT-12	2in. (5.08cm) AETB-12 / .07in. (1.78mm) BMI	TUFI	no pen., slight bump & fiber separ. on rear, slight fracture @ bond line
662	8065-2	2in. (5.08cm) AETB-8 / .07in. (1.78mm) BMI	TUFIR	penetrated - pinhole of light, 4.8mm of broken fiber
671	8066-2	2in. (5.08cm) AETB-8 / .07in. (1.78mm) BMI	TUFIR	no pen - crater to skin
670	8109-1	2in. (5.08cm) AETB-8 / .07in. (1.78mm) BMI	TUFIR	crater
675	8067-1	1in. (2.54cm) AETB-8 / .07in. (1.78mm) BMI	TUFIR	penetrated
682	8134-2	2in. (5.08cm) AETB-8 / .10in. (0.25mm) Al	RCG	crater
677	8114-1	2in. (5.08cm) AETB-8 / .10in. (0.25mm) Al	TUFI	crater
672	8109-2	2in. (5.08cm) AETB-8 / .10in. (0.25mm) Al	none	crater
669	089-2	2in. (5.08cm) AETB-12 / .07in. (1.78mm) BMI	TUFIR	penetrated
683	089-1	1.8in. (4.57cm) AETB-12 / .10in. (0.25mm) 2024 T81	TUFIR	penetrated
684	8066-1	1.8in. (4.57cm) AETB-8 / .10in. (0.25mm) 2024 T81	TUFIR	crater
673	8067-2	3in. (7.62cm) AETB-8 / .07in. (1.78mm) BMI	TUFIR	crater
674	8067-2	3in. (7.62cm) AETB-8 / .07in. (1.78mm) BMI	TUFIR	crater
652	AFRSI-1	1in. (2.54cm) nextel-AFRSI/.07iin. (1.78mm) BMI	SCOR	no pen
653	AFRSI-2	1in. (2.54cm) nextel-AFRSI/.07iin. (1.78mm) BMI	SCOR	at the penetration threshold
654	AFRSI-5	1in. (2.54cm) nextel-AFRSI/.07iin. (1.78mm) BMI	none	no pen
655	AFRSI-6	1in. (2.54cm) nextel-AFRSI/.07iin. (1.78mm) BMI	none	penetrated- large exit hole in skin ~10mm
657	TABI-1	1.058in. (2.7cm) TABI / .07in. (1.78mm) BMI	SCOR	penetrated - 10mm of broken fibers
656	TABI-2	1.178in. (3.0cm) TABI / .07in. (1.78mm) BMI	SCOR	no pen - no visible damage to skin
659	TABI-3	2.092in. (5.3cm) TABI / .07in. (1.78mm) BMI	SCOR	no pen - no visible damage to skin
658	TABI-4	2.151in. (5.5cm) TABI / .07in. (1.78mm) BMI	SCOR	no pen - no visible damage to skin
660	TABI-6	3.073in. (7.8cm)TABI / .07in. (1.78mm) BMI	SCOR	no pen - no visible damage to skin
641	641	3in. (7.62cm) AETB-20/40 / .10in. (0.25mm) 6061 T6-Al	TUFIC	No pen., no cracks, one corner broken off tile
663	2022-1	2in. (5.08cm) AETB20/20 / .10in. (0.25mm) 6061 T6-Al	TUFIC	crater
664	2048-1	3in. (7.62cm) AETB20/20 / .10in. (0.25mm) 6061 T6-Al	TUFIC	crater
665	2048-1	3in. (7.62cm) AETB20/20 / .10in. (0.25mm) 6061 T6-Al	TUFIC	crater
666	2051-1	3in. (7.62cm) AETB20/20 / .10in. (0.25mm) 6061 T6-Al	TUFIC	crater
667	2020-2	2in. (5.08cm) AETB20/20 / .10in. (0.25mm) 6061 T6-Al	RCG	crater
668	2020-1	2in. (5.08cm) AETB20/20 / .10in. (0.25mm) 6061 T6-Al	none	crater
640	S25-014	2.5in. (6.35cm) SIRCA-25 / .10in. (0.25mm) 6061 T6-Al	none	crater
643	S25-012	3in. (7.62cm) SIRCA-25 / .10in. (0.25mm) 6061 T6-Al	none	crater
645	S25-017	3in. (7.62cm) SIRCA-25 / .10in. (0.25mm) 6061 T6-Al	none	crater

APPENDIX A (continued):

Shot #	Shot Parameters			Damage Dimensions			
	Velocity (km/s)	Particle Dia. [inches/(mm)]	Mass (gms)	Ave. Hole Dia. [inches/(mm)]	Ave. Spall Dia. [inches/(mm)]	Max. Depth [inches/(cm)]	Ave. Depth [inches/(cm)]
661	6.7	1/4 (6.35)	0.3650				
678	6.7	3/32 (2.38)	0.0198	0.49 (12.45)	0.56 (14.22)	2.15 (5.46)	1.55 (3.94)
680	6.4	1/8 (3.18)	0.0453	0.53 (13.46)	0.62 (15.75)	2.53 (6.43)	2.23 (5.66)
633	6.4	3/16 (4.76)	0.1530	0.69 (17.53)	0.84 (21.34)		
634	7.1	3/16 (4.76)	0.1530	0.66 (16.76)	0.72 (18.29)		
637	7.5	3/16 (4.76)	0.1531	0.71 (18.03)	0.80 (20.32)		
638	7.1	5/32 (3.97)	0.0891	0.63 (16.00)	0.73 (18.54)		
639	7.2	1/8 (3.18)	0.0460	0.52 (13.21)	0.62 (15.75)		
623	6.2	1/4 (6.35)	0.3655	0.72 (18.29)	0.84 (21.34)		
628	8.1	3/16 (4.76)	0.1525	0.68 (17.27)	0.81 (20.51)		
629	7.5	7/32 (5.56)	0.2445	0.68 (17.27)	0.82 (20.83)		
626	6.2	3/16 (4.76)	0.1529	0.61 (15.49)	0.69 (17.53)		
662	7.0	3/16 (4.76)	0.1528	0.80 (20.32)	1.16 (29.46)		
671	6.6	1/8 (3.18)	0.0454	0.61 (15.49)	0.82 (20.83)	2.00 (5.08)	2.00 (5.08)
670	6.5	1/16 (1.59)	0.0059	0.43 (10.92)	0.58 (14.73)	1.00 (2.54)	0.96 (2.44)
675	7.1	5/32 (3.97)	0.0894				
682	6.8	1/16 (1.59)	0.0059	0.15 (3.81)	0.22 (5.59)	1.07 (2.72)	0.97 (2.46)
677	6.7	1/16 (1.59)	0.0059	0.32 (8.13)	0.55 (13.97)	0.99 (2.51)	0.98 (2.49)
672	6.6	1/16 (1.59)	0.0060	0.08 (2.03)	no spall	1.33 (3.38)	1.23 (3.12)
669	7.1	7/32 (5.56)	0.2452				
683	7.4	15/64 (5.95)	0.3094				
684	6.9	3/32 (2.38)	0.0198	0.55 (13.97)	0.76 (19.30)	1.66 (4.22)	1.46 (3.71)
673	6.5	3/32 (2.38)	0.0199	0.51 (12.95)	0.79 (20.07)	1.83 (4.65)	1.38 (3.51)
674	6.5	1/8 (3.18)	0.0456	0.61 (15.49)	0.87 (22.10)	2.72 (6.91)	2.02 (5.13)
652	6.7	1/16 (1.59)	0.0056	0.19 (4.83)	5/8x1/4 (15.88x6.35)		
653	6.8	3/32 (2.38)	0.0195	1/4x3/16 (6.35x4.76)	1/2x3/8 (12.7x9.53)		
654	6.6	1/16 (1.59)	0.0058	0.13 (3.30)	n/a		
655	6.7	1/8 (3.18)	0.0458	0.19 (4.83)	n/a		
657	6.5	1/8 (3.18)	0.0456	0.19 (4.83)	1/2x1/2 (12.7x12.7)		
656	6.3	3/32 (2.38)	0.0196	1/8x3/16 (3.18x4.76)	3/8x1/2 (9.53x12.7)		
659	6.4	5/32 (3.97)	0.0887	0.19 (4.83)	3/8x7/16 (9.53x11.11)		
658	6.8	1/8 (3.18)	0.0455	0.19 (4.83)	3/8x1/2 (9.53x12.7)		
660	6.7	1/16 (1.59)	0.0058	1/8x1/16 (3.18x1.59)	1/4x3/8 (6.35x9.53)		
641	7.3	1/8 (3.18)	0.0459	0.48 (12.19)	0.53 (13.46)	1.83 (4.65)	1.59 (4.04)
663	6.9	1/8 (3.18)	0.0458	0.48 (12.19)	0.69 (17.53)	1.70 (4.32)	1.49 (3.78)
664	6.7	1/16 (1.59)	0.0058	0.22 (5.59)	0.29 (7.37)	0.75 (1.91)	0.66 (1.68)
665	6.6	3/16 (4.76)	0.1530	0.59 (14.99)	0.79 (20.07)	2.59 (6.58)	2.56 (6.50)
666	6.8	1/4 (6.35)	0.3655	0.74 (18.80)	0.84 (21.34)	3.00 (7.62)	3.00 (7.62)
667	6.8	1/8 (3.18)	0.0458	0.41 (10.41)	1.46 (37.08)	1.70 (4.32)	1.64 (4.17)
668	6.8	1/8 (3.18)	0.0459	0.24 (6.35)	no spall	1.76 (4.47)	1.70 (4.32)
640	7.3	1/8 (3.18)	0.0460	0.61 (15.49)	0.97 (24.64)	1.56 (3.96)	1.35 (3.43)
643	7.2	3/16 (4.76)	0.1533	0.87 (22.10)	1.66 (42.16)	2.10 (5.33)	1.92 (4.88)
645	6.9	1/4 (6.35)	0.3658	1.40 (35.56)	2.70 (68.58)	2.68 (6.81)	2.36 (5.99)

REPORT DOCUMENTATION PAGE

Form Approved
OMB No. 0704-0188

1. AGENCY USE ONLY *(Leave blank)*	2. REPORT DATE	3. REPORT TYPE AND DATES COVERED
	October 1998	Technical Memorandum

4. TITLE AND SUBTITLE

Results of Two-Stage Light-Gas Gun Developmewnt Efforts and Hypervelocity Impact Tests of Advanced Thermal Protection Materials

5. FUNDING NUMBERS

RTOP 242-80-01

6. AUTHOR(S)

Charles J. Cornelison and Eric T. Watts*

7. PERFORMING ORGANIZATION NAME(S) AND ADDRESS(ES)

Ames Research Center
Moffett Field, CA 94035-1000

*The Boeing Company
Long Beach, CA 90846

8. PERFORMING ORGANIZATION REPORT NUMBER

A9811760

9. SPONSORING/MONITORING AGENCY NAME(S) AND ADDRESS(ES)

National Aeronautics and Space Administration
Washington, DC 20546-0001

10. SPONSORING/MONITORING AGENCY REPORT NUMBER

NASA/TM-1998-112234

11. SUPPLEMENTARY NOTES

Point of Contact: Charles J. Cornelison, Ames Research Center, 237-A, Moffett Field, CA 94035-1000
(650) 604-3443

12a. DISTRIBUTION/AVAILABILITY STATEMENT

Unclassified-Unlimited
Subject Category – 14

Availability: NASA CASI (301) 621-0390

12b. DISTRIBUTION CODE

Distribution: Standard

13. ABSTRACT ***(Maximum 200 words)***

Gun development efforts to increase the launching capabilities of the NASA Ames 0.5-inch two-stage light-gas gun have been investigated. A gun performance simulation code was used to guide initial parametric variations and hardware modifications, in order to increase the projectile impact velocity capability to 8 km/s, while maintaining acceptable levels of gun barrel erosion and gun component stresses. Concurrent with this facility development effort, a hypervelocity impact testing series in support of the X-33/RLV program was performed in collaboration with Rockwell International. Specifically, advanced thermal protection system materials were impacted with aluminum spheres to simulate impacts with on-orbit space debris. Materials tested included AETB-8, AETB-12, AETB-20, and SIRCA-25 tiles, tailorable advanced blanket insulation (TABI), and high temperature AFRSI (HTA). The ballistic limit for several Thermal Protection System (TPS) configurations was investigated to determine particle sizes which cause threshold TPS/structure penetration. Crater depth in tiles was measured as a function of impact particle size. The relationship between coating type and crater morphology was also explored. Data obtained during this test series was used to perform a preliminary analysis of the risks to a typical orbital vehicle from the meteoroid and space debris environment.

14. SUBJECT TERMS

Hypervelocity, Impact, Thermal Protection Materials

15. NUMBER OF PAGES

28

16. PRICE CODE

A03

17. SECURITY CLASSIFICATION OF REPORT	18. SECURITY CLASSIFICATION OF THIS PAGE	19. SECURITY CLASSIFICATION OF ABSTRACT	20. LIMITATION OF ABSTRACT
Unclassified	Unclassified		